Controlled growth of supported ZnO inverted nanopyramids with downward pointing tips

Controlled growth of supported ZnO inverted nanopyramids with downward pointing tips

Davide Barreca,[‡] *Giorgio Carraro,*[†] *Chiara Maccato,*[†]* *Thomas Altantzis,*[§] *Kimmo Kaunisto,*[#,X] *and Alberto Gasparotto*[†]*

[‡] CNR-ICMATE and INSTM, Department of Chemical Sciences, Padova University, 35131 Padova, Italy.

[†] Department of Chemical Sciences, Padova University and INSTM, 35131 Padova, Italy.

[§] EMAT, University of Antwerp, 2020 Antwerpen, Belgium.

[#] Department of Chemistry and Bioengineering, Tampere University of Technology, 33101 Tampere, Finland.

[X] VTT Technical Research Centre of Finland Ltd, 33101 Tampere, Finland.

RECEIVED DATE (to be automatically inserted after your manuscript is accepted if required according to the journal that you are submitting your paper to)

ABSTRACT

High purity porous ZnO nanopyramids with controllable properties are grown on their tips on Si(100) substrates by means of a catalyst-free vapor phase deposition route in a wet oxygen reaction environment. The system degree of preferential [001] orientation, as well as nanopyramid size, geometrical shape and density distribution, can be finely tuned by varying the growth temperature between 300 and 400°C, whereas higher temperatures lead to more compact systems with a three-dimensional (3D) morphology. A growth mechanism of the obtained ZnO nanostructures based on a self-catalytic vapor-solid (VS) mode is proposed, in order to explain the evolution of nanostructure morphologies as a function of the adopted process conditions. The results obtained by a thorough chemico-physical characterization enable to get an improved control over the properties of ZnO nanopyramids grown by this technique. Taken together, they are of noticeable importance not only for fundamental research on ZnO nanomaterials with controlled nano-organization, but also to tailor ZnO functionalities in view of various potential applications.

KEYWORDS: ZnO; nanopyramids; vapor deposition; growth mechanism, photolumiscence.

INTRODUCTION

ZnO, a biosafe II-VI semiconductor with a wide band gap (E_G = 3.4 eV),[1-8] low cost and remarkable stability,[9-13] has been the subject of an ever increasing interest since the 1930s, with a research peak at the end of the seventies.[14] This flourishing attention has been stimulated by the unique zinc oxide properties,[15-20] including the large exciton binding energy (60 meV)[1-2,21-23] and the spontaneous piezoelectric polarization,[24-29] due to the stacking of alternating O^{2-} and Zn^{2+} planes along the *c* axis of the hexagonal *wurtzite* structure.[11,30-35]

The tailoring of zinc oxide chemical, physical and functional properties as a function of the size and shape of ZnO building blocks offers a huge possibility for a variety of technological end-uses.[34,36-40] The latter encompass, among others, transparent conducting oxides,[9,14,41] (photo)catalysts for various processes,[35-36,42-45] light emitting diodes[2,46] and lasers,[30,39] electrodes for dye-sensitized[1,17,23,47] and photoelectrochemical cells,[5,36,48-50] nanostructured films with for anti-fogging and self-cleaning applications,[30,38,51-52] as well as nanoscale transducers, field emitters, resonators[1,13,16,53] and solid state gas sensors.[11,22,46] Therefore, various preparation routes[15,26,28,54-55] (from wet chemical approaches,[33,42,45,53,56] to hydrothermal/solvothermal processes,[15,22,44,50,57] electrodeposition,[5,54,58] atomic layer deposition,[40,59] chemical vapor deposition (CVD)[17,19-20,28,41] and evaporation[15,37,47,49]) have been proposed to fabricate ZnO-based systems with tailored morphologies and dimensional scales from micro to nano-level, with the aim of increasing their performances.[1,46] In this regard, beside morphology, the defect content and active area significantly affect the properties of ZnO nanomaterials for a variety of technological applications.[11,46,50,60-61]

The huge renaissance experienced by zinc oxide research from the mid-1990s has been stimulated by the possibility of growing a wide range of low-dimensional nanosystems

(including, but not limited to, nanowires, nanotubes, nanobelts, nanorings, nanosprings, hierarchical architectures and so on),[3,10,31,36,43,55] demonstrating that ZnO exhibits the richest variety of morphologies among inorganic materials.[9,61] Nonetheless, despite ZnO nanostructures have been investigated extensively up to date, the growth of materials with tuned spatial organization, high surface area and porosity is still not completely satisfactory[19,58] and represents an important challenge for modern material science.[15,45,54] In particular, the preparation of supported ZnO nanoarchitectures with precise structure and shape control, as well as the understanding of their growth mechanism, may open up new directions towards the introduction of novel properties and functionalities and meet the requirements of next-generation device fabrication.[57] In this regard, most of the work done so far has concerned arrays of 1D ZnO systems grown on specific substrates[8,10,47,49-50,53,57] whereas relatively few papers have reported on the growth of ZnO pyramids and cone-shaped structures, although the latter are highly desirable for many applications.[18,33,37] To date, the obtainment of ZnO-based nanopyramids has been most reported in a powdered form,[7,11,21,25,35,56] whereas only a few reports have described their fabrication as supported systems with upward pointing tips[13,37,62] and a very high density on the growth substrate.[18,23] Nevertheless, supported systems stand as a more attractive choice for functional applications, thanks to the lower tendency to sintering and/or deactivation and to the possibility of being directly integrated into functional devices.[4,51-52]

In this work, we report on the successful fabrication of ZnO nanopyramids with downward pointing tips without the use of any seed/buffer/catalyst layer, at variance with previous reports on the growth of ZnO nanomaterials.[4,6,27,53-54,57] The target pyramids have been obtained by a simple one-step chemical vapor deposition (CVD) route, which, beside the scalable advantages due to its industrial character, enables a high control on the purity, crystallinity and morphology

of the resulting ZnO nanostructures.[1,26] The system chemical composition, structure, nano-organization and optical properties were characterized as a function of the adopted deposition temperature, a key parameter enabling to finely tailor the system features. The experimental findings and growth mechanism presented and discussed in this work for the obtained ZnO nanostructures might shed light on the physical insights governing the shape-controlled formation of ZnO nanosystems.[16,26] To the best of our knowledge, the present work reports the first example appeared so far in the literature for the CVD of ZnO nanopyramids protruding from the substrate surface with their tips.

EXPERIMENTAL SECTION

Synthesis. ZnO depositions were performed in a home-made thermal-CVD apparatus consisting of a tubular furnace equipped with a quartz tube reactor.[48] In each experiment, $Zn(hfa)_2$•TMEDA (hfa = 1,1,1,5,5,5-hexafluoro-2,4-pentanedionate; TMEDA = *N*,*N*,*N*',*N*'-tetramethylethylenediamine), adopted as Zn precursor,[29] was placed in an external glass vessel and heated at 80°C by means of an oil bath and transported into the reaction chamber by means of electronic grade N_2 (flow rate = 100 sccm). The gas lines connecting the precursor vessel and the reactor were heated at 120°C throughout each growth experiment, in order to avoid detrimental condensation phenomena. An auxiliary electronic grade oxygen flow (rate = 30 sccm) was introduced separately into the reaction chamber after passing through a water reservoir maintained at 30ºC. Depositions were performed on *p*-type Si(100) substrates (MEMC®, Merano, Italy, 15 mm × 15 mm × 1 mm), subjected to a previously described pre-cleaning procedure.[63] The total pressure was set to 3.0 mbar, and the CVD process carried out for 120 min adopting deposition temperatures (T_d) between 300 and 500°C.

Characterization. Glancing incidence X-ray diffraction (GIXRD) patterns were recorded at a fixed incidence angle of 1.0° by means of a Bruker D8 Advance diffractometer equipped with a Göbel mirror, using a CuKα X-ray source powered at 40 kV and 40 mA.

X-ray photoelectron spectroscopy (XPS) analyses were carried out by a Perkin-Elmer Φ 5600ci instrument using a standard MgKα radiation (hν = 1253.6 eV), at working pressures < 10^{-8} mbar. The element binding energy (BE) values (uncertainty = ±0.2 eV) were corrected for charging effects by assigning a position of 284.8 eV to the C1s signal arising from adventitious contamination.[64] Atomic percentages (at. %) were calculated through peak integration, using standard PHI V5.4A sensitivity factors. Ar^+ sputtering was carried out at 3.5 kV, with an argon partial pressure of 5×10^{-8} mbar. The Zn Auger parameter was calculated as previously reported.[28,48]

Field emission-scanning electron microscopy (FE-SEM) images were collected using a Zeiss SUPRA 40 VP apparatus. Plane-view and cross-sectional micrographs were recorded with a primary beam voltage of 10 kV. The mean nanoaggregate size and deposit thickness values were estimated by using the ImageJ® (http://imagej.nih.gov/ij/, accessed September 2017) picture analyzer software. Growth rates as a function of deposition temperatures were calculated by dividing the measured thickness values (in nm) by the adopted deposition time (in min).

Cross-sectional samples suitable for transmission electron microscopy (TEM) observations were prepared by an initial mechanical polishing, using an Allied Multiprep System with diamond-lapping films, down to a thickness of approximately 20 μm, followed by Ar^+ ion milling by using a Leica EM RES102 apparatus, with acceleration voltages up to 4 kV and incident beam angles between 6° and 11°. Low and high magnification high angle annular dark field-scanning transmission electron microscopy (HAADF-STEM) images and energy dispersive X-ray

spectroscopy (EDXS) elemental maps were acquired using an aberration corrected cubed FEI Titan electron microscope operated at 300 kV, equipped with the ChemiSTEM system.[65] A probe convergence semi-angle and a detector collection inner semi-angle of 21 mrad and 55 mrad, respectively, were used for image acquisition.

Room temperature photoluminescence (PL) measurements were carried out by a Fluorolog-3 (SPEX Inc.) spectrometer with an excitation wavelength of 330 nm. Fluorescence spectra were measured at 90º to the excitation beam and were corrected by using a correction function supplied by the manufacturer.

RESULTS AND DISCUSSION

The chemico-physical properties of ZnO samples were investigated as a function of the adopted growth temperature, a parameter playing a crucial role in determining the characteristics of the fabricated nanomaterials.[29,59] The system phase composition and crystallinity were investigated by GIXRD analyses (Figure 1). As a general trend, the observed diffraction peaks displayed a high intensity and a narrow spectral width, confirming the high phase purity and good crystalline nature of the obtained nanosystems.[54] All the observed reflections could be indexed according to the hexagonal ZnO *wurtzite* ($P6_3mc$) crystal structure (a = 3.249 Å; c = 5.206 Å).[11-12,43,54,66] Under the adopted preparation conditions, the minimum temperature for the obtainment of crystalline *wurtzite* was 300°C, since preliminary growth processes at lower temperatures did not yield any appreciable diffraction peak. All the patterns were characterized by the presence of a main reflection at 2ϑ = 34.4°, corresponding to (002) ZnO planes. A comparison of the relative signal intensities with respect to those of the reference powder spectrum indicated an appreciable [001] preferential orientation, as often reported for *wurtzite* ZnO nanosystems.[17,24-25,40,47,62]. Calculation of the ratios between (002) and (101) signal intensities indicated that the highest

orientation degree occurred for samples deposited at intermediate temperatures (350–400°C, see Supporting Information (SI), Figure S1), the ones also characterized by the higher growth rates (SI, Figure S2). As can be observed in Figure 1, for the same specimens the (100) reflection intensity became negligible, and, in particular, it was completely absent for a deposition temperature of 400°C, the sample presenting the highest [001] orientation degree. This observation suggested that the majority of nanopyramids were perpendicular to the substrate surface, in line with TEM results (see below).

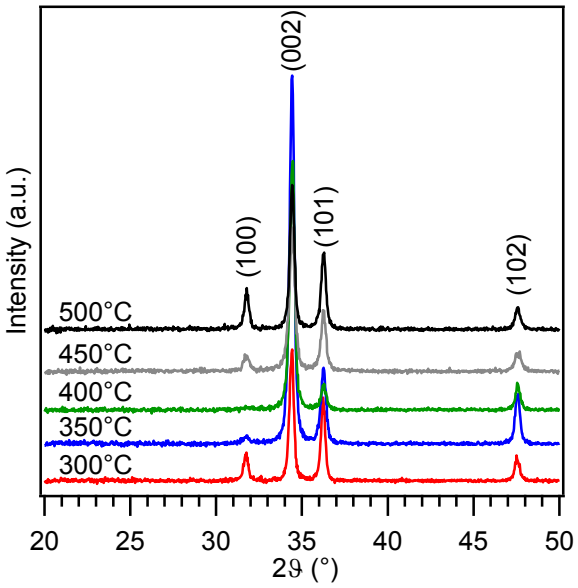

Figure 1. GIXRD patterns of ZnO nanosystems synthesized at different growth temperatures.

The surface chemical composition of the target ZnO nanomaterials was investigated by XPS. Figure S2, SI shows wide-scan surface XPS spectra of selected ZnO systems, which were dominated by zinc and oxygen photopeaks. Carbon presence (typically < 20 at.%) was attributed to adventitious surface contamination due to atmospheric exposure, since the C1s signal fell to noise level after a few minutes of Ar^+ sputtering. Irrespective of the process conditions, the

$Zn2p_{3/2}$ (Figure 2a) and Zn3p positions (BE = 1021.8 and 88.9 eV, respectively) were in line with literature values for

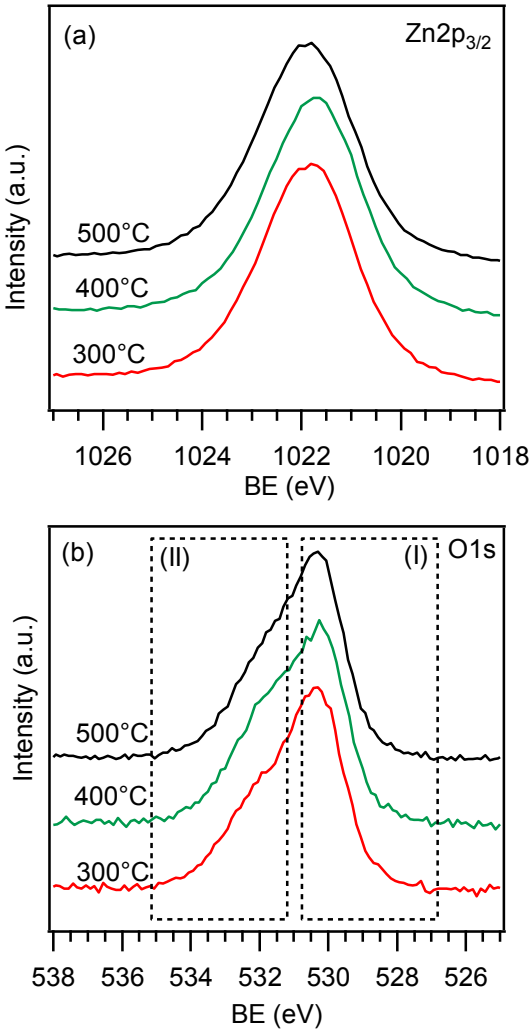

Figure 2. Surface $Zn2p_{3/2}$ (a) and O1s (b) photoelectron peaks for representative ZnO systems synthesized at different growth temperatures. In each case, the spectral intensity has been normalized for comparison purposes.

pure ZnO.[5,28,58] The finger print of zinc(II) oxide occurrence was provided by the evaluation of the Auger α parameter (α = 2010.3 eV), in excellent agreement with previous literature data.[64,67] The surface O1s signal (Figure 2b) resulted from two concurrent contributions: (I), located at BE

= 530.3 eV and attributed to Zn-O-Zn bondings of the oxide phase; (II), centered at BE = 531.9 eV, assigned to surface –OH groups, whose presence is typically observed on a ZnO surfaces.[5,64] Accordingly, the O/Zn surface ratio (typically close to 1.3) was slightly higher than 1, the value expected for stoichiometric ZnO.

A first insight into the system morphology was gained by plane-view and cross-sectional FE-SEM micrographs (Figure 3), that revealed a significant evolution of the material nano-organization as a function of the growth temperature. For $T_d \leq 400°C$, the specimens displayed an anisotropic growth, characterized by nanoyramidal aggregates with tips pointing towards the substrate surface. These nanopyramid arrays are characterized by a high homogeneity and an appreciable porosity. A detailed inspection of these micrographs confirmed that the base of the pyramids is very close to a regular hexagon, as recently reported for powdered ZnO synthesized by solution approaches[11,24,34,42,45] and for supported ZnO systems obtained by CVD.[19] Upon increasing the growth temperature ($T_d > 400°C$), the system underwent a progressive densification, leading to a lamellar texture at 450°C and, ultimately, to a globular morphology at 500°C, in line with the progressive decrease of the [001] orientation testified by XRD analyses (see above and Figure S1, SI). Correspondingly, the film thickness, after achieving a maximum value of (260±50) nm for $T_d = 350°C$, decreased down to (60±5) nm for $T_d = 500°C$. Figure S3, SI reports the Arrhenius plot of the obtained growth rates, whose maximum value occurred at $T_d = 350$ °C (≈ 2 nm/min). In particular, for $T_d < 350°C$ a surface reaction limited regime took place,[68] whereas for $T_d \geq 350°C$ the increased thermal energy supply promoted the formation of a higher number of nucleation sites at expenses of deposition on the already formed ones. As a result, thinner nanodeposits with more densely packed grains are indeed observed.[29]

The influence of the deposition temperature (T_d) on the material morphology can be further

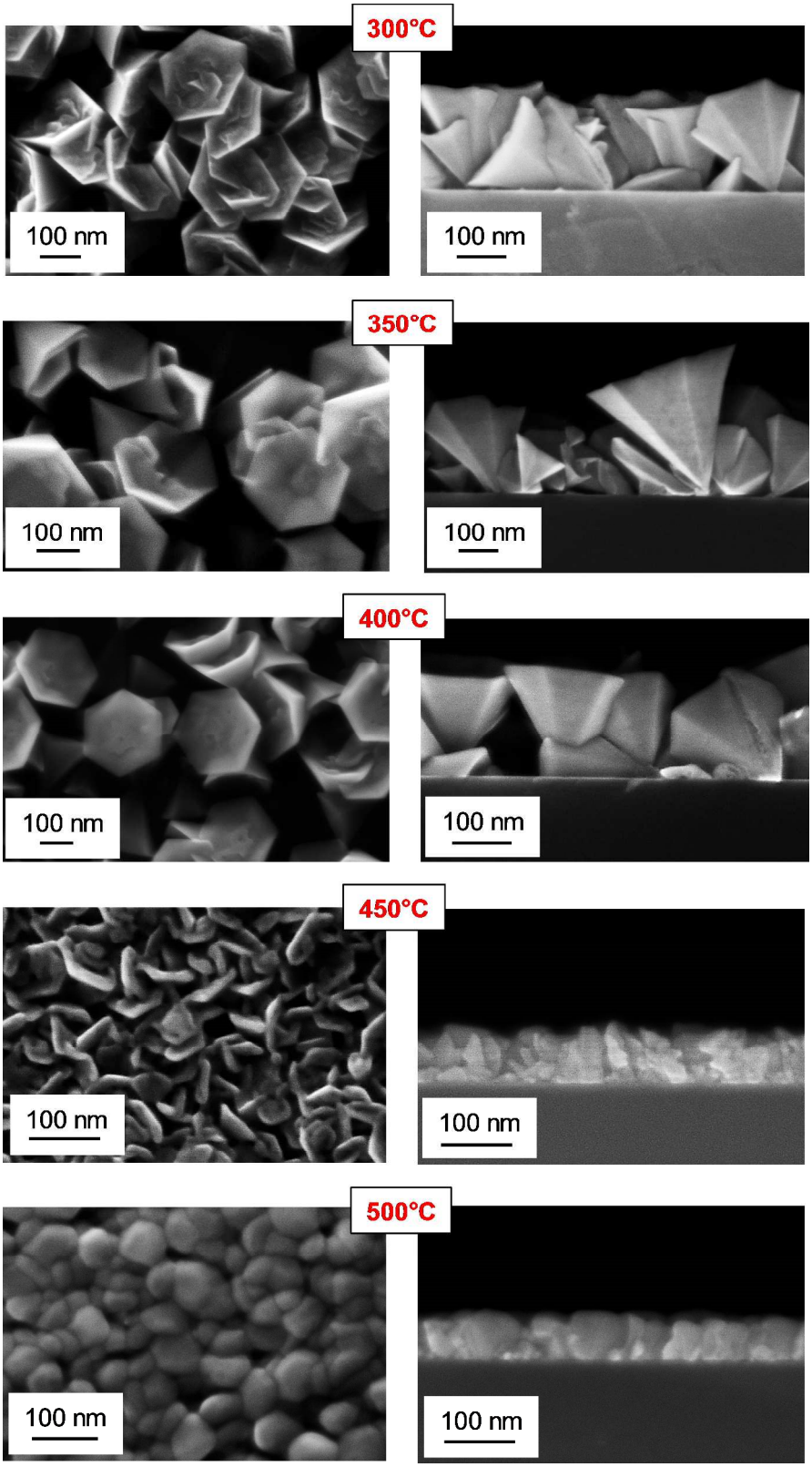

Figure 3. Plane-view and cross-sectional FE-SEM micrographs for ZnO nanosystems fabricated at different growth temperatures.

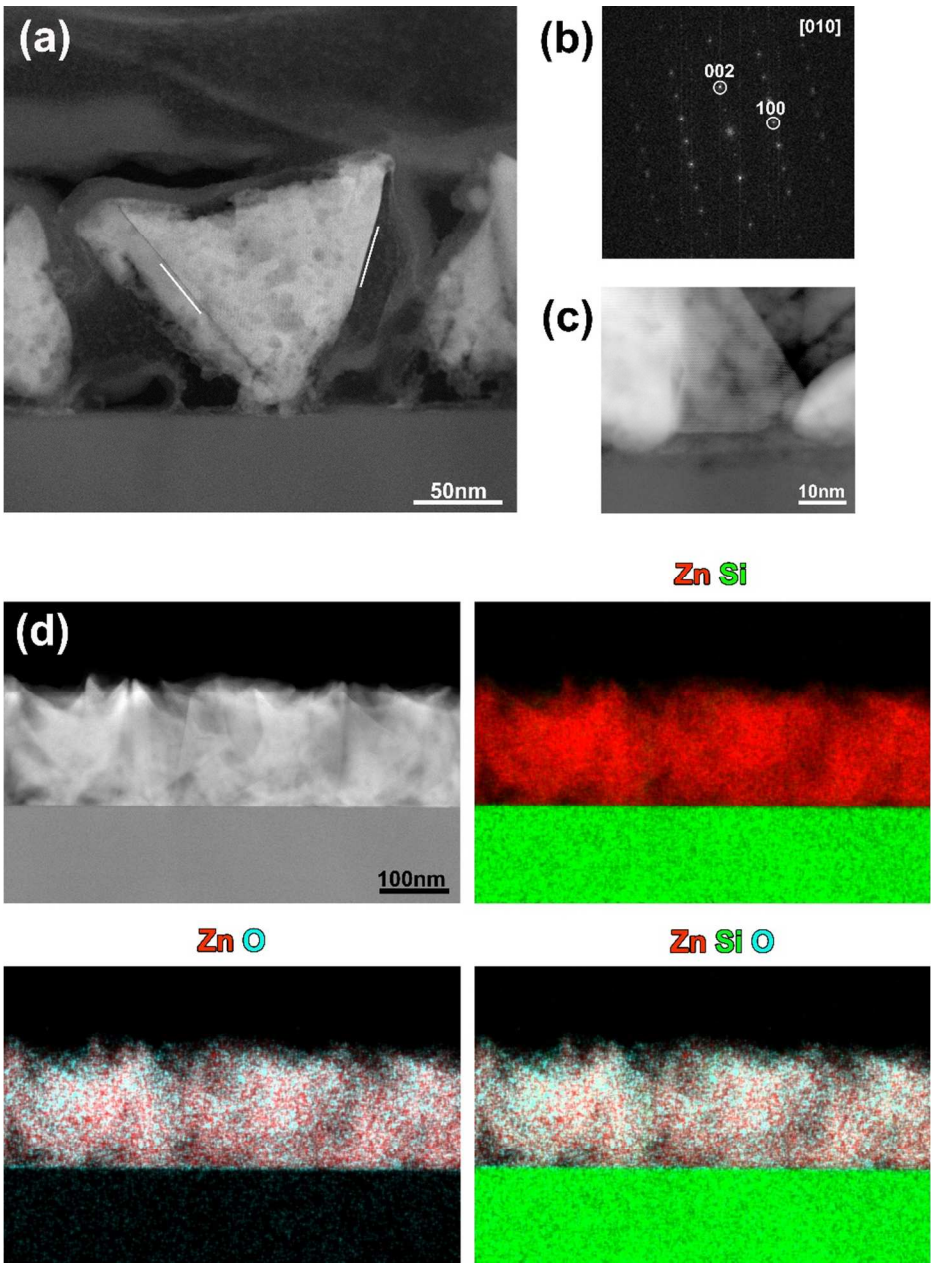

Figure 4. TEM characterization of a ZnO sample fabricated at 300°C. (a) High resolution HAADF-STEM image of a ZnO crystal, oriented along the [010] zone axis.[66] The exposed {101} facets are indicated by the white lines. (b) Fourier transform (FT) pattern of the crystal in (a). (c) High resolution HAADF-STEM micrograph of a part of a ZnO crystal. (d) HAADF-STEM image and corresponding EDXS elemental maps revealing the elemental distribution.

investigated by using the zone model proposed by Movchan and Demchishin.[68] In particular, the

calculation of the homologous temperature $T_h = T_d/T_m$ (T_m, ZnO melting temperature = 2248 K), yielded the following T_h values: 0.25 (T_d = 300°C), 0.28 (T_d = 350°C), 0.30 (T_d = 400°C), 0.32 (T_d = 450°C) and 0.34 (T_d = 500°C). The observed morphologies are in line with the model predictions, according to which porous columnar structures are expected for T_h values below 0.3. On the other hand, upon increasing the growth temperature up to 500°C, the occurrence of a denser deposit is in good agreement with model prediction of coalesced grains.

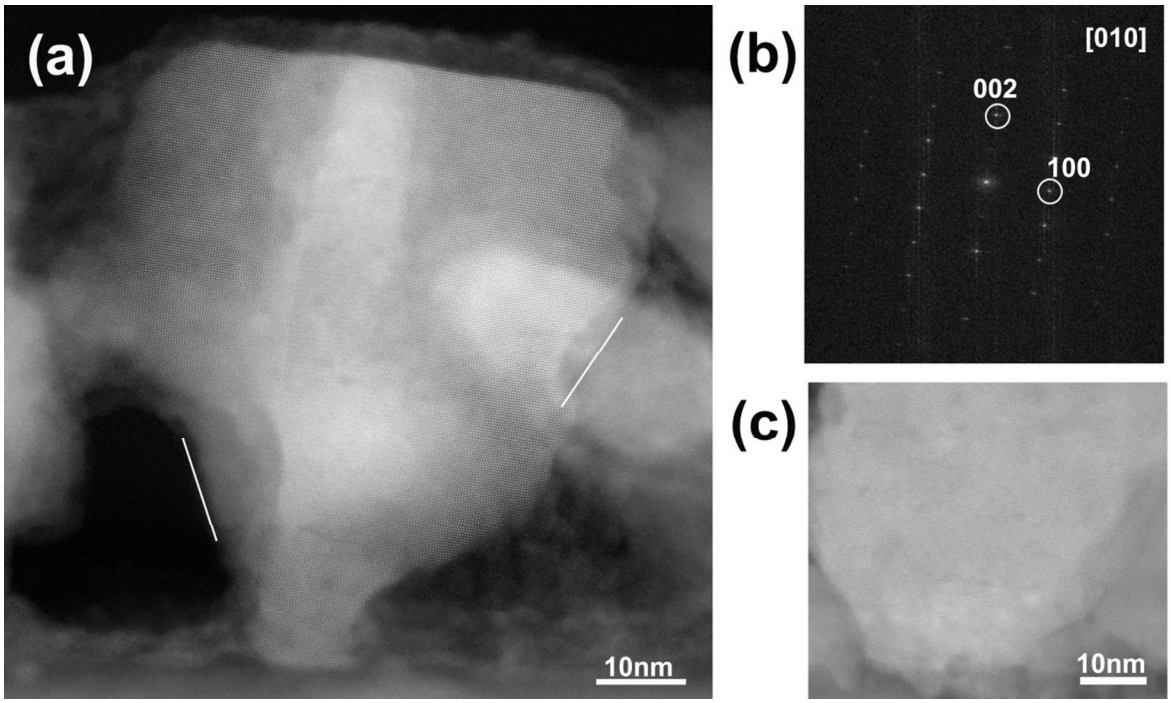

Figure 5. TEM characterization of a ZnO specimen fabricated at 400°C. (a) High resolution HAADF-STEM image of a ZnO crystal, oriented along the [010] zone axis.[66] The exposed {101} facets are indicated by the white lines. (b) FT pattern of the region in (a). (c) High resolution HAADF-STEM micrograph of a part of a ZnO crystal.

In order to investigate in detail the system structure at the nanoscale, HAADF-STEM and EDXS analyses were carried out on selected specimens fabricated at T_d = 300°C and 400°C. Figures 4 and 5 display HAADF-STEM (*Z*-contrast) overview images of both samples in cross-section,

together with EDXS elemental maps for Si, Zn and O, revealing the Si//ZnO stacking. Low magnification STEM images show that the nanopyramids characterizing the two deposits have a different height, and in particular 200 and 70 nm for the specimens grown at T_d = 300 and 400°C, respectively. The presence of dark-contrast voids in the ZnO crystals (see Figures 4a and 5a), highlights a certain system porosity.

The pertaining Fourier transforms (FTs) of the crystals (Figures 4b and 5b) could be indexed according to the hexagonal ZnO phase,[66] in line with the previously discussed XRD data. Figures 4c and 5c report higher magnification images, highlighting that most of ZnO crystals are oriented along the [010] zone axis, with the [001] orientation being almost perpendicular to the substrate. For both samples, the exposed lateral facets are the {101} ones (compare Figures 4a and 5a).

Basing on the obtained data, a schematic representation of the main structural features of the ZnO pyramids on the Si substrate is presented in Figure 6.

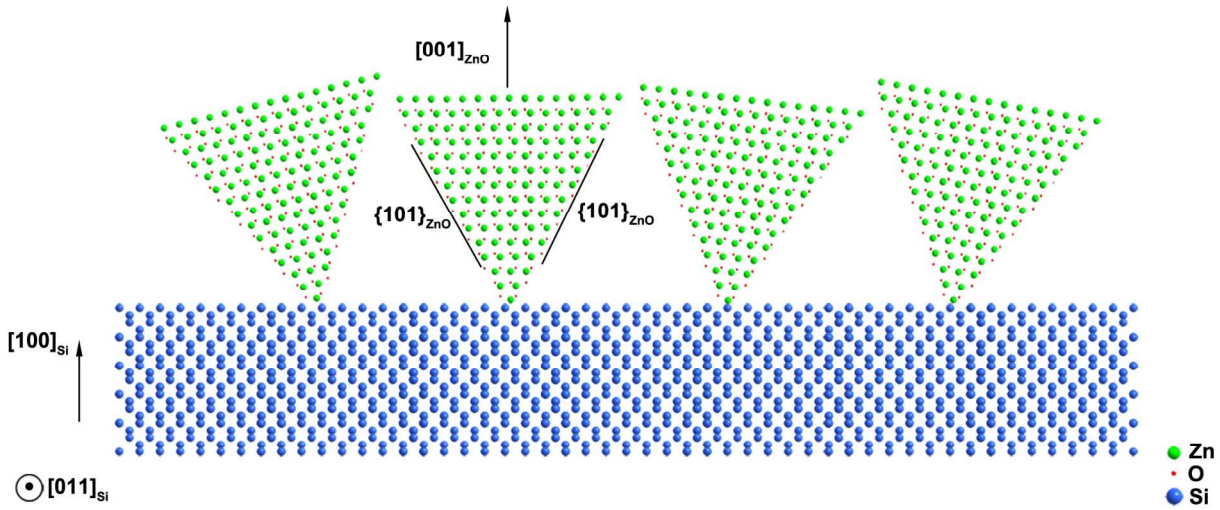

Figure 6. Schematic representation of the main structural features of ZnO pyramid arrays. The pyramidal ZnO structures are grown with their [001] axis almost perpendicular to the Si(100) surface and the exposed {101} facets are marked by the black lines in one of the pyramids.

A detailed literature analysis has evidenced the presence of a previous work[37] concerning the obtainment *via* an evaporation route of hexagonal pyramids with a morphology similar to the present one, despite with a less ordered orientation. The authors provide an explanation for this peculiar nano-organization, involving the synergistical occurrence of a vapor-solid (VS) mechanism and the growth according to a preferential orientation (*i.e.*, the [001] one). In a different way, the classical vapor-liquid-solid (VLS) process, typically observed in the presence of metal particles intentionally deposited on the growth surface,[69] which act as catalysts for the subsequent nucleation and growth of the target nanostructures, can be unambiguously ruled out under the adopted experimental conditions.

In the present case, the used reaction atmosphere contains water vapor, whose presence promotes the activation of the used Zn precursor (Figure 7a). In fact, hydroxyl groups arising from the dissociative chemisorption of water molecules on the growth surface favor the decomposition of the β-diketonate precursor, opening the chelate cycles and resulting in the subsequent elimination of ligands in the enolic form.[29,70] In the present case, –OH groups also promote the preferential growth of ZnO nanostructures along the *c* axis. This phenomenon can be explained by considering the *wurtzite*-type structure of zinc (II) oxide, formed alternating planes of Zn and O atoms along the *c* axis.[22,25,34] This arrangement produces a spontaneous polarization along the *c* axis, which, in turn, triggers an anisotropic growth along the [001] direction. This effect is additionally promoted by water supply during the deposition, inducing a preferential interaction of –OH groups with Zn(II) centers present on (001) surfaces, which further favor the precursor decomposition on these planes and a faster growth along this direction.

Figure 7b proposes a sketch of the decomposition mechanism of the Zn precursor in the presence of water vapor on Si(100) substrates. After the initial formation of the first nucleation centers

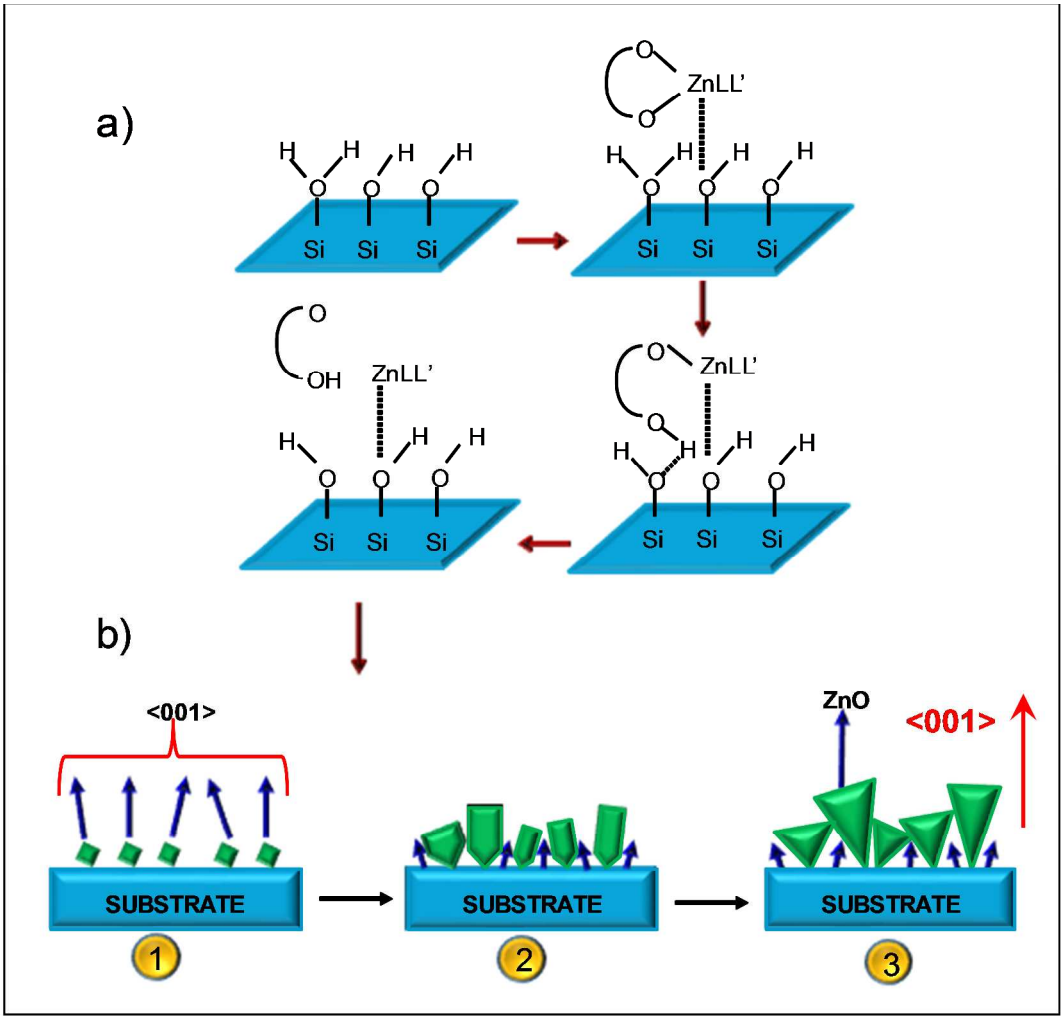

Figure 7. a) Schematic representation of the decomposition mechanism of the $Zn(hfa)_2 \bullet TMEDA$ precursor on a Si(100) substrate in a reaction environment containing water vapor. The β-diketonate and TMEDA ligand are indicated by L and L', respectively.[29] For sake of simplicity, only the elimination of one hfa ligand is shown. b) Sketch of the three steps involved in the growth of the ZnO nanopyramids obtained in the present work. The <001> orientation is marked for clarity.

(stage 1), which activate the subsequent growth process, the formation of nanostructures strongly oriented along the [001] direction (as discussed above basing on the obtained experimental results) is observed. In this regard, the pristine nuclei become progressively larger and undergo an anisotropic abnormal grain growth process,[37] resulting in the development of bullet-shaped

structures (stage 2). Such anisotropic growth can be traced back to the different crystal plane surface energy, which is much higher for (001) ones with respect to the other facets.[71]

As a consequence, [001] becomes the fastest grain growth direction, along which the bullet-shaped structures continue to grow. Subsequently (stage 3), isotropic growth becomes competitive with the above discussed anisotropic one, and ZnO pyramids are formed from the large and hexagonal top plane grown at the final stage along the [001] direction. The final results in the development of arrays of ZnO pyramids, whose packing is directly affected by the actual temperature of the growth surface. It is worthwhile highlighting that the proposed growth mechanism is indeed significantly influenced by the adopted deposition temperature. For $T \leq 400°C$, XRD analyses (see above) indicate the development of a preferential <001> orientation, which is progressively more enhanced upon going from $T = 300°C$ to $T = 400°C$. At $T > 400°C$, three-dimensional isotropic growth becomes progressively predominant with respect to the one along the [001] direction, both for the enhanced thermal energy supply and the less efficient chemisorption of water molecules, which results in a lower preferential orientation degree.[29,72] These variations are reflected by a well evident modification in the morphology of the target systems, which, at $T = 500°C$, appear as more compact three-dimensional systems.

As demonstrated by the experimental results presented so far, the obtained hexagonal pyramids possess various unique features, including: i) the uniform shape, delimited by smooth surfaces; ii) the well-defined tips, which could be promising for eventual applications in field emitters; iii) the presence of a high porosity, as evidenced by the dark-contrast voids in the above discussed TEM micrographs. The enhanced surface area nanoarrays (see also Figure S4, SI) might result to be attractive candidates for the fabrication of gas sensors and photocatalysts for a variety of end-uses.

The optical properties of ZnO nanosystems deposited at different temperatures were investigated by PL measurements (Figure 8). As can be observed, all the spectra were characterized by a prominent peak in the UV region ($\lambda \approx 380$ nm), with a remarkable tailing into the Vis region. This main contribution could be assigned to the near band-edge emission typical of ZnO, whereas the tailing was ascribed to material defectivity.[4,28,37,44] A comparative inspection of the spectra as a function of the growth temperature highlighted a slight red shift of the main peak (from 375 up to 380 nm) upon decreasing the growth temperature, along with a progressive increase of the tail magnitude, suggesting a lower optical quality and an increase of the material defectivity , which could be related to the higher degree of porosity present in the ZnO crystals grown at lower temperature.[3,58] On the other hand, the presence of surface and/or bulk defects, along with the balance between recombination/trapping of the photogenerated carriers, is known to be of utmost importance in the developed materials for gas sensing and photocatalysis.[60,73]

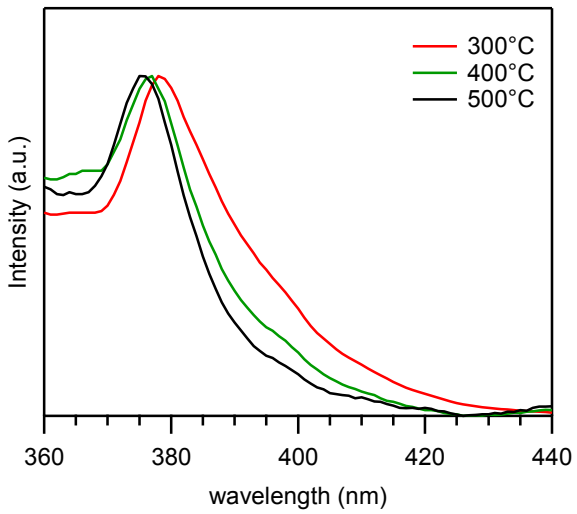

Figure 8. Representative PL spectra of ZnO specimens grown at different temperatures.

CONCLUSIONS

Arrays of supported ZnO nanopyramids with downward pointing tips and a hexagonal base were obtained on Si(100) substrates by means of a CVD process. The proposed synthetic strategy is cheap and simple with a high yield and, in principle, could be amenable for an eventual scale-up. The obtained experimental data indicated a high purity, crystallinity and optical quality for the target ZnO nanomaterials, which possess tunable morphologies as a function of the adopted growth temperature. The highest degree of <001> orientation was observed at optimal growth temperatures of 350–400°C, corresponding to the most pronounced pyramidal morphology. Detailed structural analyses enabled to propose a phenomenological growth model, based on a direction-conducting growth and a vapor-solid (VS) mechanism, directly influenced by the adopted substrate temperature.

The present results highlight how the powerful combination of complementary analytical techniques enables to investigate the complex interplay between nanosystem morphology and processing conditions. In perspective, the obtained ZnO nanopyramidal arrays are expected to provide novel insights for various potential applications, from light emitting diodes to field emitters and AFM probes, up to solid-state gas sensors and photocatalysts.

ASSOCIATED CONTENT

Supporting Information. The Supporting Information is available free of charge on the ACS Publications website at DOI: 10.1021/acs.cgd….

Experimental data on the XRD intensity ratio and growth rate as a function of the adopted deposition temperature; surface XPS wide-scan spectra; AFM analyses.

AUTHOR INFORMATION

Corresponding Authors

* chiara.maccato@unipd.it; ORCID: 0000-0001-6368-5754 (C.M.); alberto.gasparotto@unipd.it; ORCID: 0000-0003-4626-651X (A.G.).

Notes

The authors declare no competing financial interest.

ACKNOWLEDGEMENTS

This work has been supported by Padova University ex-60% 2015–2017, P-DiSC #03BIRD2016-UNIPD projects and ACTION post-doc fellowship. T. A. acknowledges a postdoctoral grant from the Research Foundation Flanders (FWO, Belgium). Thanks are also due to Dr. Rosa Calabrese (Department of Chemical Sciences, Padova University, Italy) and to Dr. T.-P. Ruoko (Department of Chemistry and Bioengineering, Tampere University of Technology, Finland) for skilful technical support.

REFERENCES

(1) Laurenti, M.; Stassi, S.; Canavese, G.; Cauda, V. Surface Engineering of Nanostructured ZnO Surfaces. *Adv. Mater. Interfaces* **2017**, *4*, 1600758.

(2) Guo, Z.; Zhao, D.; Shen, D.; Fang, F.; Zhang, J.; Li, B. Structure and Photoluminescence Properties of Aligned ZnO Nanobolt Arrays. *Cryst. Growth Des.* **2007**, *7*, 2294-2296.

(3) Shen, J.; Zhuang, H.; Wang, D.; Xue, C.; Liu, H. Growth and Characterization of ZnO Nanoporous Belts. *Cryst. Growth Des.* **2009**, *9*, 2187-2190.

(4) Ranjith, K. S.; Pandian, R.; McGlynn, E.; Rajendra Kumar, R. T. Alignment, Morphology and Defect Control of Vertically Aligned ZnO Nanorod Array: Competition between "Surfactant" and "Stabilizer" Roles of the Amine Species and Its Photocatalytic Properties. *Cryst. Growth Des.* **2014**, *14*, 2873-2879.

(5) Huang, M.-C.; Wang, T.; Wu, B.-J.; Lin, J.-C.; Wu, C.-C. Anodized ZnO Nanostructures for Photoelectrochemical Water Splitting. *Appl. Surf. Sci.* **2016**, *360*, 442-450.

(6) Lv, R.; Wang, T.; Su, F.; Zhang, P.; Li, C.; Gong, J. Facile Synthesis of ZnO Nanopencil Arrays for Photoelectrochemical Water Splitting. *Nano Energy* **2014**, *7*, 143-150.

(7) Flomin, K.; Jen-La Plante, I.; Moshofsky, B.; Diab, M.; Mokari, T. Selective Growth of Metal Particles on ZnO Nanopyramids via a One-Pot Synthesis. *Nanoscale* **2014**, *6*, 1335-1339.

(8) Arslan, O.; Abalı, Y. Controlled Modulation of 1D ZnO Nano/Micro Structures: Evaluation of the Various Effects on the Photocatalytic Activity. *J. Phys. Chem. Solids* **2017**, *108*, 88-97.

(9) Wang, Z. L. Nanostructures of Zinc Oxide. *Mater. Today* **2004**, *7*, 26-33.

(10) Wu, C. C.; Wuu, D. S.; Lin, P. R.; Chen, T. N.; Horng, R. H. Three-Step Growth of Well-Aligned ZnO Nanotube Arrays by Self-Catalyzed Metalorganic Chemical Vapor Deposition Method. *Cryst. Growth Des.* **2009**, *9*, 4555-4561.

(11) Ahmad, M. Z.; Chang, J.; Ahmad, M. S.; Waclawik, E. R.; Wlodarski, W. Non-Aqueous Synthesis of Hexagonal ZnO Nanopyramids: Gas Sensing Properties. *Sens. Actuators, B* **2013**, *177*, 286-294.

(12) Khan, R.; Hassan, M. S.; Cho, H.-S.; Polyakov, A. Y.; Khil, M.-S.; Lee, I.-H. Facile Low-Temperature Synthesis of ZnO Nanopyramid and its Application to Photocatalytic

Degradation of Methyl Orange Dye Under UV Irradiation. *Mater. Lett.* **2014**, *133*, 224-227.

(13) Chen, H.; Qi, J.; Zhang, Y.; Zhang, X.; Liao, Q.; Huang, Y. Controlled Growth and Field Emission Properties of Zinc Oxide Nanopyramid Arrays. *Appl. Surf. Sci.* **2007**, *253*, 8901-8904.

(14) Klingshirn, C. ZnO: Material, Physics and Applications. *ChemPhysChem* **2007**, *8*, 782-803.

(15) Podrezova, L. V.; Porro, S.; Cauda, V.; Fontana, M.; Cicero, G. Comparison between ZnO Nanowires Grown by Chemical Vapor Deposition and Hydrothermal Synthesis. *Appl. Phys. A* **2013**, *113*, 623-632.

(16) Kuo, C.-Y.; Ko, R.-M.; Tu, Y.-C.; Lin, Y.-R.; Lin, T.-H.; Wang, S.-J. Tip Shaping for ZnO Nanorods via Hydrothermal Growth of ZnO Nanostructures in a Stirred Aqueous Solution. *Cryst. Growth Des.* **2012**, *12*, 3849-3855.

(17) Pflitsch, C.; Nebatti, A.; Brors, G.; Atakan, B. MOCVD-Growth of Thin Zinc Oxide Films From Zinc Acetylacetonate and Air. *J. Cryst. Growth* **2012**, *348*, 5-9.

(18) Chen, S.; Wilson, R. M.; Binions, R. Synthesis of Highly Surface-Textured ZnO Thin Films by Aerosol Assisted Chemical Vapour Deposition. *J. Mater. Chem. A* **2015**, *3*, 5794-5797.

(19) Chen, C.; Yan, T.; Chou, M. M. C.; Lee, C.-Y.; Wang, B.-M.; Wen, M.-J.; Zhang, X. Self-Assembly Epitaxial Growth of Nanorods on Nanowalls in Hierarchical ZnO Hexagonal Nanocastle. *J. Nanopart. Res.* **2014**, *16*, 2142.

(20) Bekermann, D.; Gasparotto, A.; Barreca, D.; Bovo, L.; Devi, A.; Fischer, R. A.; Lebedev, O. I.; Maccato, C.; Tondello, E.; Van Tendeloo, G. Highly Oriented ZnO Nanorod Arrays by a Novel Plasma Chemical Vapor Deposition Process. *Cryst. Growth Des.* **2010**, *10*, 2011-2018.

(21) Zhang, J.; Zhu, P.; Li, J.; Chen, J.; Wu, Z.; Zhang, Z. Fabrication of Octahedral-Shaped Polyol-Based Zinc Alkoxide Particles and Their Conversion to Octahedral Polycrystalline ZnO or Single-Crystal ZnO Nanoparticles. *Cryst. Growth Des.* **2009**, *9*, 2329-2334.

(22) Wang, Z.; Xue, J.; Han, D.; Gu, F. Controllable Defect Redistribution of ZnO Nanopyramids with Exposed $\{10\bar{1}1\}$ Facets for Enhanced Gas Sensing Performance. *ACS Appl. Mater. Interfaces* **2015**, *7*, 308-317.

(23) Nicolay, S.; Benkhaira, M.; Ding, L.; Escarre, J.; Bugnon, G.; Meillaud, F.; Ballif, C. Control of CVD-Deposited ZnO Films Properties Through Water/DEZ Ratio: Decoupling of Electrode Morphology and Electrical Characteristics. *Sol. Energy Mater. Sol. Cells* **2012**, *105*, 46-52.

(24) Li, P.; Wang, D.; Wei, Z.; Peng, Q.; Li, Y. Systematic Synthesis of ZnO Nanostructures. *Chem. Eur. J.* **2013**, *19*, 3735-3740.

(25) Chen, Y.; Zeng, D.; Zhang, K.; Lu, A.; Wang, L.; Peng, D.-L. Au-ZnO Hybrid Nanoflowers, Nanomultipods and Nanopyramids: One-Pot Reaction Synthesis and Photocatalytic Properties. *Nanoscale* **2014**, *6*, 874-881.

(26) Montenegro, D. N.; Souissi, A.; Martínez-Tomás, C.; Muñoz-Sanjosé, V.; Sallet, V. Morphology Transitions in ZnO Nanorods Grown by MOCVD. *J. Cryst. Growth* **2012**, *359*, 122-128.

(27) Ghosh, M.; Ghosh, S.; Seibt, M.; Rao, K. Y.; Peretzki, P.; Mohan Rao, G. Ferroelectric Origin in One-Dimensional Undoped ZnO Towards High Electromechanical Response. *CrystEngComm* **2016**, *18*, 622-630.

(28) Bekermann, D.; Ludwig, A.; Toader, T.; Maccato, C.; Barreca, D.; Gasparotto, A.; Bock, C.; Wieck, A. D.; Kunze, U.; Tondello, E.; Fischer, R. A.; Devi, A. MOCVD of ZnO Films from *Bis*(Ketoiminato)Zn(II) Precursors: Structure, Morphology and Optical Properties. *Chem. Vap. Deposition* **2011**, *17*, 155-161.

(29) Barreca, D.; Ferrucci, A. P.; Gasparotto, A.; Maccato, C.; Maragno, C.; Tondello, E. Temperature-Controlled Synthesis and Photocatalytic Performance of ZnO Nanoplatelets. *Chem. Vap. Deposition* **2007**, *13*, 618-625.

(30) Shaban, M.; Zayed, M.; Hamdy, H. Nanostructured ZnO Thin Films for Self-Cleaning Applications. *RSC Adv.* **2017**, *7*, 617-631.

(31) Wang, Z. L. Self-Assembled Nanoarchitectures of Polar Nanobelts/Nanowires. *J. Mater. Chem.* **2005**, *15*, 1021-1024.

(32) Kong, X. Y.; Ding, Y.; Yang, R.; Wang, Z. L. Single-Crystal Nanorings Formed by Epitaxial Self-Coiling of Polar Nanobelts. *Science* **2004**, *303*, 1348-1351.

(33) Chang, Y.-C.; Yang, W.-C.; Chang, C.-M.; Hsu, P.-C.; Chen, L.-J. Controlled Growth of ZnO Nanopagoda Arrays with Varied Lamination and Apex Angles. *Cryst. Growth Des.* **2009**, *9*, 3161-3167.

(34) Javon, E.; Gaceur, M.; Dachraoui, W.; Margeat, O.; Ackermann, J.; Saba, M. I.; Delugas, P.; Mattoni, A.; Bals, S.; Van Tendeloo, G. Competing Forces in the Self-Assembly of Coupled ZnO Nanopyramids. *ACS Nano* **2015**, *9*, 3685-3694.

(35) Cargnello, M.; Sala, D.; Chen, C.; D'Arienzo, M.; Gorte, R. J.; Murray, C. B. Structure, Morphology and Catalytic Properties of Pure and Alloyed Au-ZnO Hierarchical Nanostructures. *RSC Adv.* **2015**, *5*, 41920-41922.

(36) Sun, Y.; Chen, L.; Bao, Y.; Zhang, Y.; Wang, J.; Fu, M.; Wu, J.; Ye, D. The Applications of Morphology Controlled ZnO in Catalysis. *Catalysts* **2016**, *6*, 188.

(37) Tian, Y.; Lu, H.-B.; Li, J.-C.; Wu, Y.; Fu, Q. Synthesis, Characterization and Photoluminescence Properties of ZnO Hexagonal Pyramids by the Thermal Evaporation Method. *Physica E* **2010**, *43*, 410-414.

(38) Myint, M. T. Z.; Kumar, N. S.; Hornyak, G. L.; Dutta, J. Hydrophobic/Hydrophilic Switching on Zinc Oxide Micro-textured Surface. *App. Surf. Sci.* **2013**, *264*, 344-348.

(39) Barreca, D.; Bekermann, D.; Devi, A.; Fischer, R. A.; Gasparotto, A.; Maccato, C.; Tondello, E.; Rossi, M.; Orlanducci, S.; Terranova, M. L. Novel Insight Into the Alignment and Structural Ordering of Supported ZnO Nanorods. *Chem. Phys. Lett.* **2010**, *500*, 287-290.

(40) Krajewski, T. A.; Terziyska, P.; Luka, G.; Lusakowska, E.; Jakiela, R.; Vlakhov, E. S.; Guziewicz, E. Diversity of Contributions Leading to the Nominally *n*–type Behavior of ZnO Films Obtained by Low Temperature Atomic Layer Deposition. *J. Alloys Compd.* **2017**, *727*, 902-911.

(41) Faÿ, S.; Kroll, U.; Bucher, C.; Vallat-Sauvain, E.; Shah, A. Low Pressure Chemical Vapour Deposition of ZnO Layers for Thin-Film Solar Cells: Temperature-Induced Morphological Changes. *Sol. Energy Mater. Sol. Cells* **2005**, *86*, 385-397.

(42) Li, P.; Wei, Z.; Wu, T.; Peng, Q.; Li, Y. Au−ZnO Hybrid Nanopyramids and Their Photocatalytic Properties. *J. Am. Chem. Soc.* **2011**, *133*, 5660-5663.

(43) Wei, Y.; Huang, Y.; Wu, J.; Wang, M.; Guo, C.; Qiang, D.; Yin, S.; Sato, T. Synthesis of Hierarchically Structured ZnO Spheres by Facile Methods and their Photocatalytic deNOx Properties. *J. Hazard. Mater.* **2013**, *248*, 202-210.

(44) Kayaci, F.; Vempati, S.; Ozgit-Akgun, C.; Biyikli, N.; Uyar, T. Enhanced Photocatalytic Activity of Homoassembled ZnO Nanostructures on Electrospun Polymeric Nanofibers: A Combination of Atomic Layer Deposition and Hydrothermal Growth. *Appl. Catal., B* **2014**, *156*, 173-183.

(45) Kim, S.; Kim, M.; Kim, T.; Baik, H.; Lee, K. Evolution of Space-Efficient and Facet-Specific ZnO 3-D Nanostructures and Their Application in Photocatalysis. *CrystEngComm* **2013**, *15*, 2601-2607.

(46) Morandi, S.; Fioravanti, A.; Cerrato, G.; Lettieri, S.; Sacerdoti, M.; Carotta, M. C. Facile Synthesis of ZnO Nano-Structures: Morphology Influence on Electronic Properties. *Sens. Actuators, B* **2017**, *249*, 581-589.

(47) Lu, L.; Chen, J.; Li, L.; Wang, W. Direct Synthesis of Vertically Aligned ZnO Nanowires on FTO Substrates using a CVD Method and the Improvement of Photovoltaic Performance. *Nanoscale Res. Lett.* **2012**, *7*, 293.

(48) Barreca, D.; Carraro, G.; Gasparotto, A.; Maccato, C.; Altantzis, T.; Sada, C.; Kaunisto, K.; Ruoko, T.-P.; Bals, S. Vapor Phase Fabrication of Nanoheterostructures Based on ZnO for Photoelectrochemical Water Splitting. *Adv. Mater. Interfaces* **2017**, *4*, 1700161.

(49) Zhong, M.; Sato, Y.; Kurniawan, M.; Apostoluk, A.; Masenelli, B.; Maeda, E.; Ikuhara, Y.; Delaunay, J.-J. ZnO Dense Nanowire Array on a Film Structure in a Single Crystal Domain Texture for Optical and Photoelectrochemical Applications. *Nanotechnology* **2012**, *23*, 495602.

(50) Chen, H.; Wei, Z.; Yan, K.; Bai, Y.; Zhu, Z.; Zhang, T.; Yang, S. Epitaxial Growth of ZnO Nanodisks with Large Exposed Polar Facets on Nanowire Arrays for Promoting Photoelectrochemical Water Splitting. *Small* **2014**, *10*, 4760-4769.

(51) Barreca, D.; Gasparotto, A.; Maccato, C.; Tondello, E.; Štangar, U. L.; Patil, S. R. Photoinduced Superhydrophilicity and Photocatalytic Properties of ZnO Nanoplatelets. *Surf. Coat. Technol.* **2009**, *203*, 2041-2045.

(52) Bekermann, D.; Gasparotto, A.; Barreca, D.; Devi, A.; Fischer, R. A.; Kete, M.; Lavrenčič Štangar, U.; Lebedev, O. I.; Maccato, C.; Tondello, E.; Van Tendeloo, G. ZnO

Nanorod Arrays by Plasma-Enhanced CVD for Light-Activated Functional Applications. *ChemPhysChem* **2010**, *11*, 2337-2340.

(53) Wrobel, G.; Piech, M.; Gao, P.-X.; Dardona, S. Direct Synthesis of ZnO Nanorod Field Emitters on Metal Electrodes. *Cryst. Growth Des.* **2012**, *12*, 5051-5055.

(54) Kıcır, N.; Tüken, T.; Erken, O.; Gumus, C.; Ufuktepe, Y. Nanostructured ZnO Films in Forms of Rod, Plate and Flower: Electrodeposition Mechanisms and Characterization. *Appl. Surf. Sci.* **2016**, *377*, 191-199.

(55) Zhou, Y.; Zhang, J.; Zhang, B.; Qiang, L.; Da, Y.; Su, G.; Li, J. Spontaneous Symmetry breaking Discovers the Formation of Aeroplane-Like ZnO Nanocrystals. *Appl. Phys. Lett.* **2014**, *104*, 121901.

(56) Kuang, Q.; Zhou, X.; Zheng, L.-S. Hexagonal ZnO/SnO_2 Core-Shell Micropyramids: Epitaxial Growth-Based Synthesis, Chemical Conversion, and Cathodoluminescence. *Inorg. Chem. Front.* **2014**, *1*, 186-192.

(57) Lee, W. W.; Yi, J.; Kim, S. B.; Kim, Y.-H.; Park, H.-G.; Park, W. I. Morphology-Controlled Three-Dimensional Nanoarchitectures Produced by Exploiting Vertical and In-Plane Crystallographic Orientations in Hydrothermal ZnO Crystals. *Cryst. Growth Des.* **2011**, *11*, 4927-4932.

(58) Wu, K.; Sun, Z.; Cui, J. Unique Approach toward ZnO Growth with Tunable Properties: Influence of Methanol in an Electrochemical Process. *Cryst. Growth Des.* **2012**, *12*, 2864-2871.

(59) Guziewicz, E.; Przezdziecka, E.; Snigurenko, D.; Jarosz, D.; Witkowski, B. S.; Dluzewski, P.; Paszkowicz, W. Abundant Acceptor Emission from Nitrogen-Doped ZnO Films Prepared by Atomic Layer Deposition under Oxygen-Rich Conditions. *ACS Appl. Mater. Interfaces* **2017**, *9*, 26143-26150.

(60) Lupan, O.; Postica, V.; Gröttrup, J.; Mishra, A. K.; de Leeuw, N. H.; Carreira, J. F. C.; Rodrigues, J.; Ben Sedrine, N.; Correia, M. R.; Monteiro, T.; Cretu, V.; Tiginyanu, I.; Smazna, D.; Mishra, Y. K.; Adelung, R. Hybridization of Zinc Oxide Tetrapods for Selective Gas Sensing Applications. *ACS Appl. Mater. Interfaces* **2017**, *9*, 4084-4099.

(61) Gasparotto, A.; Barreca, D.; Maccato, C.; Tondello, E. Manufacturing of Inorganic Nanomaterials: Concepts and Perspectives. *Nanoscale* **2012**, *4*, 2813-2825.

(62) Alimanesh, M.; Rouhi, J.; Hassan, Z. Broadband Anti-Reflective Properties of Grown ZnO Nanopyramidal Structure on Si Substrate via Low-Temperature Electrochemical Deposition. *Ceram. Int.* **2016**, *42*, 5136-5140.

(63) Barreca, D.; Gasparotto, A.; Maccato, C.; Tondello, E.; Lebedev, O. I.; Van Tendeloo, G. CVD of Copper Oxides from a β-Diketonate Diamine Precursor: Tailoring the Nano-Organization. *Cryst. Growth Des.* **2009**, *9*, 2470-2780.

(64) Moulder, J. F.; Stickle, W. F.; Sobol, P. E.; Bomben, K. D., *Handbook of X-ray photoelectron spectroscopy*. Perkin Elmer Corporation, Eden Prairie, MN, USA: 1992.

(65) Schlossmacher, P.; Klenov, D. O.; Freitag, B.; von Harrach, H. S. Enhanced Detection Sensitivity with a New Windowless XEDS System for AEM Based on Silicon Drift Detector Technology. *Microsc. Today* **2010**, *18*, 14-20.

(66) Pattern N° 36-1451, JCPDS (2000).

(67) http://srdata.nist.gov/xps.

(68) Jensen, K. F., *Chemical Vapor Deposition: Principles and Applications*. Academic Press, London,: 1993.

(69) Xia, Y.; Yang, P.; Sun, Y.; Wu, Y.; Mayers, B.; Gates, B.; Yin, Y.; Kim, F.; Yan, H. One-Dimensional Nanostructures: Synthesis, Characterization, and Applications. *Adv. Mater.* **2003**, *15*, 353-389.

(70) Armelao, L.; Barreca, D.; Bottaro, G.; Gasparotto, A.; Tondello, E.; Ferroni, M.; Polizzi, S. Innovative Approaches to Oxide Nanosystems: CeO_2-ZrO_2 Nanocomposites by a Combined PE-CVD/Sol–Gel Route. *Chem. Vap. Deposition* **2004**, *10*, 257-264.

(71) Feng, Z. C., *Handbook of Zinc Oxide and Related Materials: Volume 2, Devices and Nano-Engineering*. CRC Press 2012.

(72) Park, W. I. Controlled Synthesis and Properties of ZnO Nanostructures Grown by Metalorganic Chemical Vapor Deposition: A Review. *Met. Mater. Int.* **2008**, *14*, 659.

(73) Carraro, G.; Maccato, C.; Gasparotto, A.; Montini, T.; Turner, S.; Lebedev, O. I.; Gombac, V.; Adami, G.; Van Tendeloo, G.; Barreca, D.; Fornasiero, P. Enhanced Hydrogen Production by Photoreforming of Renewable Oxygenates Through Nanostructured Fe_2O_3 Polymorphs. *Adv. Funct. Mater.* **2014**, *24*, 372.

For Table of Contents Use Only

Controlled growth of supported ZnO inverted nanopyramids with downward pointing tips

Davide Barreca, Giorgio Carraro, Chiara Maccato,* Thomas Altantzis, Kimmo Kaunisto, and Alberto Gasparotto*

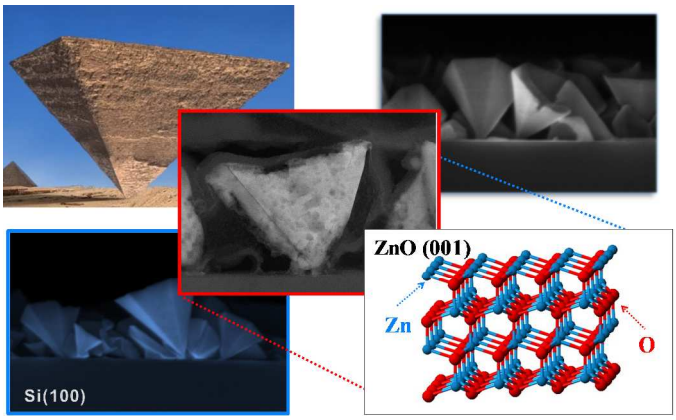

The fabrication of supported ZnO nanopyramids with hexagonal bases and downward pointing tips is performed by a catalyst-free vapor phase process. A possible growth mechanism is proposed to explain the formation of the target structures under the adopted conditions. The system morphology can be finely tuned through controlled variations of the growth temperature, a key result for eventual technological applications.